Cui et al. *Zool. Res.* 2021, 42(5): 637−649
https://doi.org/10.24272/j.issn.2095-8137.2021.126

ZR | Zoological Research

Article Open Access

Role of juvenile hormone receptor *Methoprene-tolerant 1* in silkworm larval brain development and domestication

Yong Cui[1,#], Zu-Lian Liu[2,#], Cen-Cen Li[3,#], Xiang-Min Wei[1], Yong-Jian Lin[1], Lang You[2], Zi-Dan Zhu[1], Hui-Min Deng[1], Qi-Li Feng[1,*], Yong-Ping Huang[2,*], Hui Xiang[1,*]

[1] *Guangdong Provincial Key Laboratory of Insect Developmental Biology and Applied Technology*, *Guangzhou Key Laboratory of Insect Development Regulation and Application Research*, *Institute of Insect Science and Technology*, *School of Life Sciences*, *South China Normal University*, *Guangzhou*, *Guangdong* 510631, *China*

[2] *Key Laboratory of Insect Developmental and Evolutionary Biology*, *Institute of Plant Physiology and Ecology*, *Shanghai Institutes for Biological Sciences*, *Chinese Academy of Sciences*, *Shanghai* 200032, *China*

[3] *College of Life Sciences*, *Xinyang Normal University*, *Xinyang*, *Henan* 464000, *China*

ABSTRACT

The insect brain is the central part of the neurosecretory system, which controls morphology, physiology, and behavior during the insect's lifecycle. Lepidoptera are holometabolous insects, and their brains develop during the larval period and metamorphosis into the adult form. As the only fully domesticated insect, the Lepidoptera silkworm *Bombyx mori* experienced changes in larval brain morphology and certain behaviors during the domestication process. Hormonal regulation in insects is a key factor in multiple processes. However, how juvenile hormone (JH) signals regulate brain development in Lepidoptera species, especially in the larval stage, remains elusive. We recently identified the JH receptor *Methoprene tolerant 1* (*Met1*) as a putative domestication gene. How artificial selection on *Met1* impacts brain and behavioral domestication is another important issue addressing Darwin's theory on domestication. Here, CRISPR/Cas9-mediated knockout of *Bombyx Met1* caused developmental retardation in the brain, unlike precocious pupation of the cuticle. At the whole transcriptome level, the ecdysteroid (20-hydroxyecdysone, 20E) signaling and downstream pathways were overactivated in the mutant cuticle but not in the brain. Pathways related to cell proliferation and specialization processes, such as extracellular matrix (ECM)-receptor interaction and tyrosine metabolism pathways, were suppressed in the brain. Molecular evolutionary analysis and *in vitro* assay identified an amino acid replacement located in a novel motif under positive selection in *B. mori*, which decreased transcriptional binding activity. The *B. mori* MET1 protein showed a changed structure and dynamic features, as well as a weakened co-expression gene network, compared with *B.*

Received: 26 July 2021; Accepted: 26 August 2021; Online: 27 August 2021

Foundation items: This work was supported by the National Natural Science Foundation of China (32070411, 31720103916, 31330071, 31672494), Natural Science Foundation of Guangdong Province (2019A1515011012), and Strategic Priority Research Program of the Chinese Academy of Sciences (XDB11010600)

#Authors contributed equally to this work

*Corresponding authors, E-mail: qlfeng@scnu.edu.cn; yphuang@sibs.ac.cn; xiang_shine@foxmail.com

mandarina. Based on comparative transcriptomic analyses, we proposed a pathway downstream of JH signaling (i.e., tyrosine metabolism pathway) that likely contributed to silkworm larval brain development and domestication and highlighted the importance of the biogenic amine system in larval evolution during silkworm domestication.

Keywords: *Met1*; Brain; Artificial selection; Tyrosine metabolism pathway; Silkworm;

INTRODUCTION

The insect brain is the central part of the neurosecretory system, which controls morphology, physiology, and behavior during the insect's lifecycle. Lepidoptera are holometabolous insects, which experience brain development during the larval period and metamorphosis. Larval brain size increases after each molt and brain morphology changes markedly during metamorphosis, including the differentiation of optic lobes, antennal lobes, and mushroom bodies (Champlin & Truman, 1998).

Two key insect hormones, i.e., juvenile hormone (JH) and ecdysteroid (20-hydroxyecdysone, 20E), orchestrate insect growth, molting, metamorphosis, and reproduction via their receptors and responsive genes (Liu et al., 2018). JH prevents 20E-induced larval-pupal/adult metamorphosis until insects reach the appropriate stage and is therefore referred to as the "status quo" hormone (Daimon et al., 2012, 2015; Liu et al., 2018). In many insect species, Methoprene-tolerant (Met), a member of the basic helix-loop-helix-Per-Arnt-Sim transcription factor family, functions as a JH receptor and positively regulates the expression of the JH-responsive gene *Krüppel homolog 1* (*Kr-h1*) (Daimon et al., 2015; Li et al., 2019; Zhu et al., 2019). During the larval stages, *Kr-h1* represses the pupal-specifier gene *Broad-complex* (*Br-C*) (Kayukawa et al., 2016) as well as the adult-specifier gene *Ecdysone-induced protein 93* (*E93*) (Kayukawa et al., 2017), which can be induced by 20E, to prevent precocious larval-pupal or larval-adult transition.

The mechanism of JH regulation varies among tissues and species. For example, recent advances indicate that in the reproductive system, the role of JH cannot be explained simply as "status-quo" in many tissues and the role of JH signaling shows notably variation among species (Li et al., 2019; Riddiford, 2020; Shpigler et al., 2020). In the brain, studies on *Drosophila* indicate that depletion of JH or knockout of its receptors can repress optic lobe proliferation and cause premature abnormalities in the organization of optic lobe neuropils during larval-pupal transition (Abdou et al., 2011; Riddiford et al., 2010). In these studies, the precocious appearance of the ecdysone receptor (EcR) or expression of its responsive gene (*Br-C*) was detected, suggesting that JH is required for the development of the nervus opticus and the prevention of 20E signaling in the brain (Abdou et al., 2011; Riddiford et al., 2010). JH also drives the maturation of spontaneous mushroom body neural activity and behavior in adult *Drosophila* (Leinwand & Scott, 2021). Similar functions have also been found in hemimetabolous house crickets (Cayre et al., 1994, 2005).

The role of JH/JH signaling in Lepidoptera brain development is still largely unknown compared with the role of ecdysone, which is reported to induce cell proliferation during optic lobe neurogenesis in the moth *Manduca sexta* (Champlin & Truman, 1998). Recent research showed that application of a potent JH analogue in 5th instar silkworm larvae stimulates the division of brain neurosecretory cells, thereby implying that JH plays a role in the functional development of the silkworm brain (Tanriverdi & Yelkovan, 2020). This raises the question of whether (and how) JH signaling regulates brain development in Lepidoptera species. In the current study, we used the domestic silkworm *Bombyx mori* as a model and performed CRISPR/Cas9-mediated knockout of the JH receptor *Met1*. We then conducted comparative transcriptome analyses in the brain and epidermis to decipher possible features of JH signaling in the brain.

Bombyx mori is a fully domesticated insect and *Met1* has been identified as a candidate domestication gene (Xiang et al., 2018), thus providing a good opportunity the address the functional impact of the JH receptor from an evolutionary view. Similar to the decrease in brain size reported in some domesticated animals (Agnvall et al., 2017; Stuermer & Wetzel, 2006), *B. mori* also shows a "simpler" larval brain, with weak brain lobe fusion and smaller relative brain volume compared with its wild ancestor *B. mandarina* (Figure 1). This suggests that artificial selection may impact the brain. In addition, like other domestic animals (Axelsson et al., 2013; Wang et al., 2016), selection on brain and behavior, mediated by the neuronal system (Pennisi, 2011), is reported to have occurred during silkworm domestication (Xiang et al., 2018). In regard to behavior, *B. mori* shows increased hyperphagia, reduced locomotor activity, loss of escape response, and greater tolerance to human handling compared with *B. mandarina* (Mignon-Grasteau et al., 2005; Nusinovich et al., 2017). Given that JH may influence insect behavior patterns through regulation of brain neurogenesis and neural activity as well as neurotransmitter signaling (Leinwand et al., 2021; Sasaki et al., 2012; Wheeler et al., 2015), this raises the

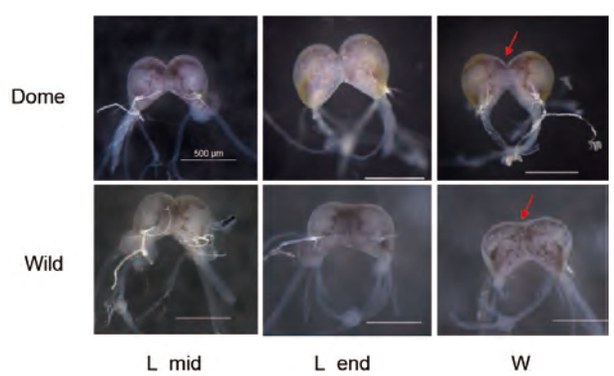

Figure 1 Comparison of brain morphology in *B. mori* and *B. mandarina* at larval stage

Dome: *B. mori* brain. Wild: *B. mandarina* brain. L_mid: Middle of final larval stage. L_end: Final day of final larval stage. W: Wandering stage. Scale bars: 500 μm. Arrows indicate degree of connection between two brain globes.

question of whether (and how) artificial selection of the JH receptor *Met1* influenced changes in the brain and behavior during silkworm domestication. Thus, we conducted evolutionary and functional analyses of amino acid replacement in *B. mori* and performed comprehensive brain transcriptome analyses between *B. mori* and *B. mandarina*.

Our results showed that unlike preventing precocious metamorphosis of the cuticle, JH signals mediated by *Met1* potentially promoted silkworm larval brain development, without obvious repression of pupal- and adult-specifier genes. Furthermore, two JH downstream signaling pathways, i.e., tyrosine metabolism and extracellular matrix (ECM)-receptor interaction pathways, likely contributed to silkworm larval brain development. Artificial selection of *Met1* fixed two nonsynonymous sites specific in *B. mori*, which affected protein structure and weakened transcriptional binding activity and the co-expression network of *Met1*. In addition, the biogenic amine system may be involved in the changes in larval behavior during silkworm domestication.

MATERIALS AND METHODS

Silkworm strains

Domestic (*B. mori*, strain P50) and wild silkworms (*B. mandarina*) were used for all experiments and comparative transcriptomic analyses. The *B. mandarina* specimens were collected from Zhejiang Province (China) and were maintained under laboratory conditions. The multivoltine silkworm strain *Nistari* was used for CRISPR-Cas9 knockout. Larvae were reared on fresh mulberry leaves under standard conditions (Tan et al., 2013).

CRISPR-Cas9-mediated knockout of *Met1*

The target sequence was designed according to the feature of GGN19GG (Fu et al., 2014; Hwang et al., 2013). Three 23 bp sgRNA targeting sites were identified at the exon of *Met1* and were used for knockout (Supplementary Figure S1). The sgRNA DNA template was synthesized by polymerase chain reaction (PCR), with Q5® High-Fidelity DNA Polymerase (New England Biolabs, USA). One oligonucleotide (*Met1*-228-sgF1, *Met1*-563-sgF2, and *Met1*-899-sgF3), which encoded the T7 polymerase binding site, sgRNA targeting sequence, and overlap sequence, was separately annealed to a common oligonucleotide that encoded the remainder of the sgRNA sequence (sgRNA-R). The reaction conditions were the same as described previously (Cui et al., 2018).

The sgRNA was synthesized based on the DNA template *in vitro* with a MAXIscript® T7 Kit (Ambion, USA) according to the manufacturer's instructions. The transcribed sgRNA was precipitated by phenol/chloroform/isoamylol (25:24:1, pH<5.0, Solarbio, China) and by isopropanol, then quantified using a NanoDrop-2000, re-dissolved in RNase-free water to 1 000 ng/μL, and finally stored at −80 °C. The Cas9 gene template was provided by the Shanghai Institute of Plant Physiology and Ecology (China). Cas9 mRNA was prepared using a mMESSAGE mMACHINE® T7 kit (Ambion, USA) according to the manufacturer's instructions. The transcribed sgRNA was precipitated by phenol/chloroform/isoamylol (25:24:1, pH<5.0, Solarbio, China) and quantified using a NanoDrop-2000, diluted to 1 000 ng/μL in RNase-free water, and stored at −80 °C.

The *B. mori* eggs were collected and injected within 6 h after oviposition. Cas9 mRNA (1 000 ng/μL) and sgRNA (1 000 ng/μL) were mixed and injected into preblastoderm *Nistari* embryos (~12 nL/egg) using a micro-injector (FemtoJet®, Germany), according to the standard protocols. The injected eggs were incubated in a humidified chamber at 25 °C for 9–10 days until hatching.

Target site activity examination by *in vitro* DNA cleavage assay

To test the cleavage activity of selected target sites, a DNA cleavage assay as performed. A mix of 150 ng of Cas9 protein (New England Biolabs, China), 200 ng of sgRNA, 2 μL of 10×NEB buffer, and 100 ng of plasmid containing a target sequence was made and incubated at 37 °C for 1 h. After heating to inactivate Cas9 protein at 65 °C for 10 min, the reaction mixture was analyzed in 1% agarose gel.

Genomic DNA extraction and genotyping analysis

Genomic PCR and sequencing were carried out to examine the *Met1* mutation induced by the CRISPR/Cas9 system. Genomic DNA was extracted using DNA extraction buffer (2.5:1:2:2.5 ratio of 10% SDS to 5 mol/L NaCl to 0.5 mol/L EDTA to 1 mol Tris-HCl, pH=8) and incubated with 60 mg/mL proteinase K, then purified via standard phenol-chloroform and isopropanol precipitation extraction, followed by RNaseA treatment. The PCR conditions were as follows: 94 °C for 2 min, 35 cycles of 94 °C for 30 s, 57 °C for 30 s, and 72 °C for 50 s, followed by a final extension of 72 °C for 10 min. The PCR products were cloned into a pMD^{TM}19-T Vector (Takara, Japan). The primers designed to detect mutagenesis in the second targeted site are listed in Supplementary Table S1.

RNA extraction, cDNA synthesis, and quantitative real-time PCR (qRT-PCR)

The epidermis and brains of wild-type (WT) and mutant 4th instar silkworms were dissected. Total RNA was extracted using TRIzol reagent (TaKaRa, China) according to the manufacturer's instructions. After purification with phenol-chloroform, 2 μg of RNA was treated with 2 units of DNase I to remove trace amounts of genomic DNA. Reverse transcription was performed using the Reverse Transcriptase M-MLV Kit according to the manufacturer's protocols (TaKaRa, China). The primers used for amplifying *BmKr-h1* cDNA were 5'-ACCCATACTGGCGAGCGACCAT-3'(forward) and 5'-CCTC TCCTTTGTGTGAATACGACGG-3'(reverse). The primers used for cDNA amplification of *BmRp49* (internal control) were 5'-CTCCCTCGAGAAGTCCTACGAACT-3' (forward) and 5'-TGCTGGGCTCTTTCCACGA-3' (reverse). The qRT-PCR was performed under the following conditions: SYBR Premix Ex Taq (2×) (Promega, USA): 10 μL in 20 μL reaction volume; primer concentrations: 0.4 μL (10 μmol/L); immunoprecipitated DNA samples: 4 μL. The mixtures were incubated at 95 °C for 10 s, then 40 cycles at 95°C for 5 s and 60 °C for 31 s using an ABI7300 fluorescence quantitative PCR system (Applied Biosystems, USA). Error bars represent standard deviation (*SD*) of three replicates. Significant differences were analyzed by Student's *t*-test. *, **, and *** indicate false discovery rate

(FDR)-corrected P<0.05, 0.01, and 0.001, respectively.

RNA sequencing (RNA-seq) and data analysis

Three duplicate samples were set for RNA-seq of the WT and mutant epidermis and brain samples and the domestic and *B. mandarina* brain samples, respectively. The epidermis and brain samples were dissected, stored in dry ice, and then sent to the Novogene Company (China) for RNA extraction and RNA-seq. Sequencing libraries were generated using a NEBNext® UltraTM RNA Library Prep Kit for Illumina® (New England Biolabs, USA) following the manufacturer's recommendations and index codes were added to attribute sequences to each sample. Clustering of the index-coded samples was performed on a cBot Cluster Generation System using a HiSeq 4000 PE Cluster Kit (Illumina, USA) according to the manufacturer's instructions. After cluster generation, the library preparations were sequenced on the Illumina Hiseq 4000 platform (Illumina, USA) and 150 bp paired-end reads were generated.

Sequenced raw data were qualified, filtered, built, and mapped to the reference silkworm genome database (http://www.silkdb.org/silkdb/) using TopHat v2.1.1 (Trapnell et al., 2009). HTSeq v0.6.0 was used to count read numbers mapped to each gene and further normalized using DEseq2 in the R package v1.16.1 (TNLIST, China) (Anders et al., 2015; Love et al., 2014). Principal component analysis (PCA) was performed using genes expressed in the brain (normalized reads>5) with online software (https://www.omicshare.com/tools/).

Differentially expressed genes (DEGs) were identified using Cuffdiff in the package Cufflinks v2.2.1 (Ghosh & Chan, 2016), with corrected P<0.05 and $|Log_2^{fold\ change}|$>1. The expression value of each gene was calculated and normalized using fragments per kilobase of exon per million reads mapped (FPKM) (Trapnell et al., 2010). Gene ontology (GO) and Kyoto Encyclopedia of Genes and Genomes (KEGG) pathway enrichment analyses of DEGs were implemented online (https://www.omicshare.com/tools/) using all expressed genes (FPKM>1) in the brain and cuticle of the silkworm as background.

Identification of selective sweep

Based on available whole-genome single nuclear polymorphic (SNP) data of the domesticated and *B. mandarina* populations (https://doi.org/10.5061/dryad.fn82qp6), the selection signature of *Met1* was screened according to the pipeline applied in Xiang et al. (2018) (https://doi.org/10.5061/dryad.fn82qp6). Specifically, a sliding window approach with 5 kb windows sliding in 500 bp steps was applied to identify genomic regions associated with domestication. To discern selective sweeps from the potential background caused by the bottleneck effect, a very stringent threshold was set to screen out regions that significantly deviated from the overall distribution. Only those windows within the top 1% of selective signatures (corresponding P-value of Z test<0.001) and applied Fst (fixation index) between the two groups were used to represent the selective signatures, taking the highest 1% value as the cutoff. Selection in the *B. mori* group (i.e., early domesticated group) was further confirmed by limiting π at a relatively low level (lowest 5%) and reduction of diversity (ROD) ($1-\pi_{domestic}/\pi_{wild}$; representing reduction of diversity in domesticated lines). Allelic frequency and SNP annotation were calculated using in-house Perl scripts.

Examination of amino acid substitution and remodeling of 3D structure of MET1

The amino acid sequences of MET1 in *B. mori* (GenBank accession No. NM_001114986.1) were independently aligned with those of *B. mandarina* (https://doi.org/10.5061/dryad.fn82qp6), *Antheraea yamamai* (Kim et al., 2018), *Manduca sexta* (Kanost et al., 2016), *Spodoptera litura* (GenBank accession No. XP_022837764.1), *Helicoverpa armigera* (GenBank accession No. XP_021188262.1), *Plodia interpunctella* (GenBank accession No. ANZ54967.1), *Amyelois transitella* (GenBank accession No. XP_013186860.1), *Operophtera brumata* (GenBank accession No. KOB74415.1), and *Dendrolimus spectabilis* (GenBank accession No. ATB19377.1) using MEGA 6.0 (Tamura et al., 2013). To explore the structural effects of amino acid residue replacement, the 3D structures of the *B. mori* and *B. mandarina* MET1 proteins were remodeled using Protein Structure Prediction Server (PS)^2 v3.0 with default parameters (http://ps2v3.life.nctu.edu.tw/) (Huang et al., 2015). The structures were saved in PDB format and analyzed using Swiss-PdbViewer v4.0.1 (Swiss Institute of Bioinformatics, Lausanne, Switzerland) (Guex & Peitsch, 1997). With the predicted 3D structure and query sequences, the packing density of each residue was calculated by the weighted contact number (WCN) derived from protein dynamical properties (Lin et al., 2008).

Phylogenetic analysis by maximum-likelihood (PAML) on *Met1*

The rate ratio (ω) of nonsynonymous to synonymous nucleotide substitutions was estimated using PAML v4.8 (Yang, 1997). After high-quality codon alignment of the above sequences, a series of evolutionary models in the likelihood framework were compared using the species tree of the insects. One ratio model was used to detect average ω across the tree (ω0). Two ratio branch models and two ratio branch-site models were used to detect the ω of the appointed branch to test the (ω1) and ω of all other branches (ω_background). A likelihood ratio test was performed to compare the fit of the two ratio models with the one ratio model to determine whether *Met1* is rapidly evolved in the appointed branch (ω1>ω0; ω1>ω_background; P-value<0.05). The branch site model was also used to detect amino acid sites likely to be rapidly evolved in the appointed branch using Bayes Empirical Bayes (BEB) analysis (Yang et al., 2005).

Production of proteins *in vitro*

A full-length MET1 open reading frame (ORF) fragment was amplified using cDNA of the silk gland from domestic and *B. mandarina* silkworms with primers: Met-CDS-SgfI-F and Met-CDS-PmeI-R (Supplementary Figure S1 and Table S1). Obtained DNA fragments were then sub-cloned into the pF25A ICE T7 Flexi vector between the SgfI and PmeI restriction enzyme sites, generating recombinant expression vectors. The nucleic acid sequence corresponding to the

region between the two Per-Arnt-Sim (PAS) domains was truncated and sent to TSINGKE (China) for artificial synthesis. The truncated fragment was also sub-cloned into the pF25A ICE T7 Flexi vector, as described above.

Recombinant proteins were produced using the TnT T7 Insect Extract Protein Expression System (Promega, USA). Plasmid (4 μg) DNA template was added to the reaction mixture and the reaction was carried out at 29 °C for 4 h according to the manufacturer's protocols. The protein productivity of the TnT T7 Insect Extract Protein kit is ~50 μg/mL of the translation reaction mixture (Ezure et al., 2010; Golan-Mashiach et al., 2012).

Electrophoretic mobility shift assay (EMSA)

To verify differences in the DNA-protein binding capacity of MET1 to the putative E-box element sequence in the *BmKr-h1* promoter, EMSA was conducted using a LightShift Chemiluminescent EMSA Kit (Thermo Scientific, USA). The DNA oligonucleotides containing the consensus MET1 binding sites were labeled with biotin at the 5' end, incubated at 95 °C for 10 min, and annealed to generate the probe by natural cooling. Unbiotinylated probes were used as competitors to each other. The biotin-labeled oligonucleotides at the 5' end were synthesized by Invitrogen (China). The oligonucleotide probes used are shown in Supplementary Table S1.

The DNA-binding reactions were conducted in 20 μL of solution containing 150 ng of protein translated *in vitro*, 1×binding buffer, 50 ng of poly (dI-dC), 2.5% glycerol, 0.05% NP-40, 50 mmol/L KCl, 5 mmol/L $MgCl_2$, 4 mmol/L EDTA, and 20 fmol of a biotinylated end-labeled double-stranded probe for 20 min at room temperature. For the competition assay, 50- and 100-fold molar excesses of unbiotinylated double-stranded probe were added before adding the labeled probe. The gels were run at 100 V for 1.5 h using 6% polyacrylamide gel on ice. After electrophoresis, the gels were blotted onto positively charged Nylon membranes (Amersham Biosciences, USA). The membranes were then developed using the LightShift Chemiluminescent EMSA Kit according to the manufacturer's protocol.

Construction of weighted gene co-expression networks

The FPKM values of DEGs in seven silkworm developmental stages (middle of last larval instar, end of the larval instar, wandering, pre-pupal, first day of pupal, middle of pupal, newly emerged moth) were calculated and used to construct a gene co-expression network using the WGCNA package in R v3.4.4 (Langfelder & Horvath, 2008). The gene co-expression modules were identified with the following parameters: networkType="unsigned", softPower=6 (*B. mori*) and 12 (*B. mandarina*), minModuleSize=30. The soft power value was chosen as a saturation level for a soft threshold of the correlation matrix based on the criterion of approximate scale-free topology. Briefly, genes with similar patterns of connection strengths to other genes or high topological overlap (TO) were selected and clustered based on their TO values to identify gene co-expression network groups. The gene co-expression network groups including the *Met1* gene were selected to draw the networks using Cytoscape v3.6.1 (Li et al., 2017).

RESULTS

CRISPR/Cas9-mediated knockout of silkworm *Met1* retarded brain development, in contrast to precocious metamorphosis of the cuticle

The genomic structure of *Met1* was composed of one 1 545 bp long exon (Supplementary Figure S1A). After predicting the sgRNA sites (see Materials and Methods) followed by *in vitro* assay of activity of the corresponding sgRNAs (Supplementary Figure S1B), we selected one target site located at 563 bp for CRISPR/Cas9-mediated knockout. Consistent with previous research (Daimon et al., 2015), we found that 27.9% (56 of 201) of G0 larvae became severe larval-pupal mosaics during molting from the 3rd (L3) to 4th (L4) instar, with a brown-colored pupal cuticle that covered about half of the body (Figure 2A, B). Abdominal prolegs of some individuals showed degeneration (Supplementary Figure S2A). Most mosaic mutants failed to completely shed the old L3 cuticle (Supplementary Figure S2B). The homozygous mutations of *Met1* were all lethal at the end of the L2 stage (Figure 2C). Given that the role of JH and its receptor *Met1* in the silkworm early larval stage remains elusive (Daimon et al., 2015) and that the mosaic mutants showed a clear phenotype of precocious metamorphosis of the cuticle, we used these mutants for further analysis.

Unlike the precocious metamorphosis in the cuticle, the mosaic mutant brain showed developmental retardation when compared with that of the WT (Figure 2D, E). The mosaic mutant brains retained the larval status and were significantly smaller (Figure 2D, E). In addition, PCA of the brain transcriptome data showed that the PC1 axis explained 63.5% of the variance in the samples, with younger to older samples distributed from right to left (i.e., L4 for WT, L5, wandering, and pupal stages), suggesting that this axis may be negatively associated with developmental status. The mosaic mutant brains were located on the right side of the WT L4 instar and differed from those of more mature developmental stages, e.g., L5 instar, wandering, and pupal stages (Figure 2F). This pattern suggests that the mosaic mutant brains remained at the earlier larval stage or suffered from developmental problems, rather than at the stage of precocious metamorphosis.

Genotyping of the mosaic mutant cuticles and brains showed that there were diverse types of indels in the genomic region spanning the target site, most of which caused frame-shift mutations of *Met1* (Figure 2G, H). The mutation rate was 46.7%–75.0% at the individual level (data not shown). These results confirmed that the somatic mosaic mutagenesis system was equally effective in both the cuticle and brain. In the silkworm brain, *Met1* mediated JH signaling functions in normal growth and likely promoted cell proliferation. Blockade of this pathway did not seem to activate precocious metamorphosis, as found in *Drosophila* brains or other insect tissues (Abdou et al., 2011; Champlin &Truman, 1998; Daimon et al., 2015).

***Kr-h1* was repressed in the epidermis and brain, whereas *Br-C* and *E93* were overactivated in the epidermis in *Met1* mutants**

To study the molecular mechanisms underlying the differences in cuticle and brain responses to *Met1* depletion,

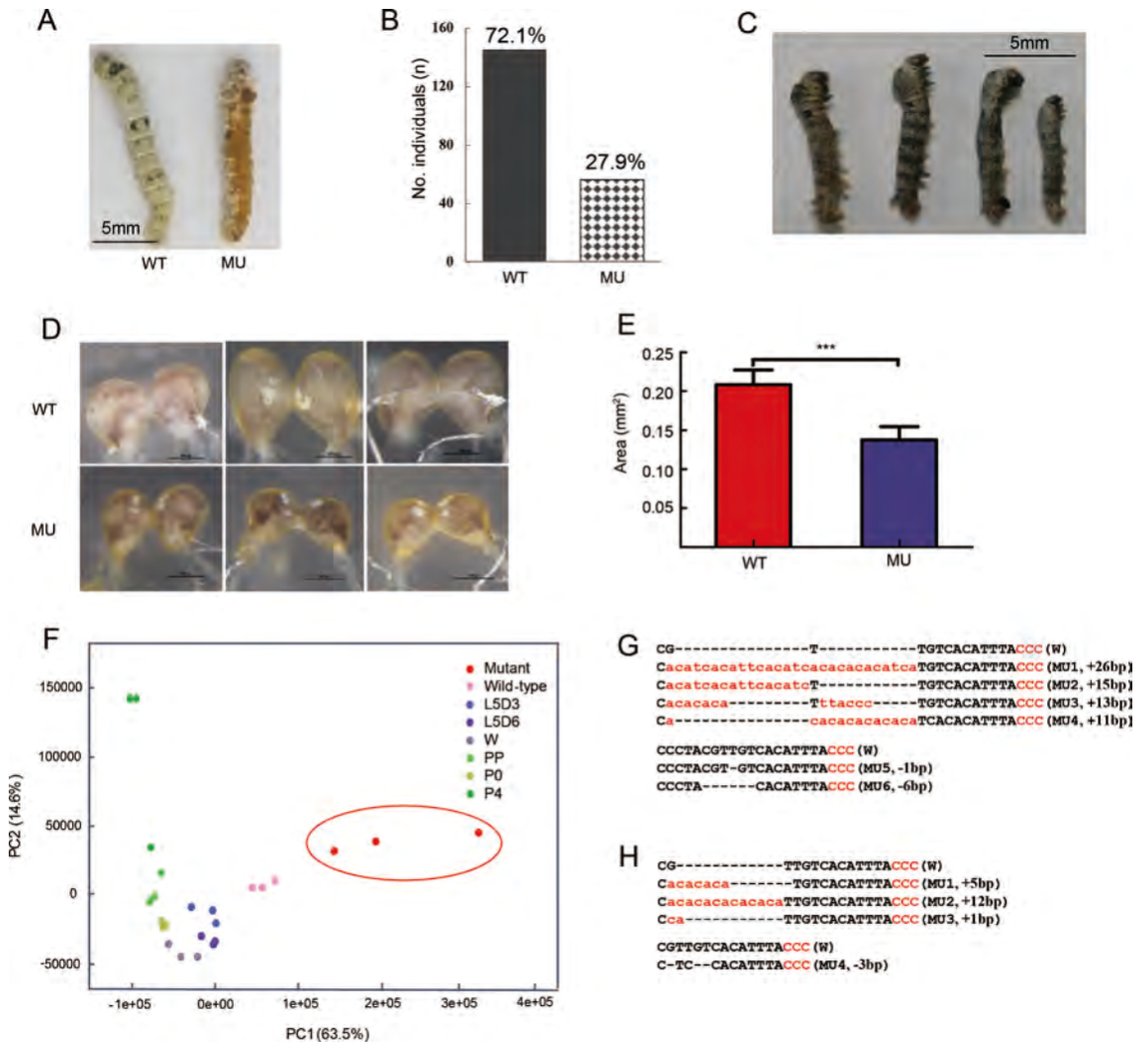

Figure 2 Phenotypes of CRISPR/Cas9-induced JH receptor mutants and *Met1* mutation impaired brain development observed by cytological and transcriptome experiments

A: Representative images of *Met1* mosaic mutants, exhibiting pupal characters at 4th larval stage. WT: Wild-type, refers to individuals from laboratory population of domestic silkworm strain *Nistari*, which were not subjected to injection; MU: Mutant. B: Sum of number of severe larval-pupal mosaics in G0 generation. C: *Met1* homozygous mutant larvae were developmentally arrested and most died during molt from 2nd to 3rd larval stages. Scale bar: 5 mm. D: MU larval brain retained its larval status and was smaller in size compared with WT. Scale bar: 200 μm. E: Comparison of brain size between WT and MU (n=6). Error bar: *SD*; ***: P<0.001, by t-test. Brain area was calculated by ImageJ2 software. F, G: Various types of insertion mutations screened from mosaic brain and cuticle, indicating high loss-of-function mutation rates in mosaics. Deletions are indicated by hyphens and insertions are shown by red lowercase letters. CCC: PAM sequences. H: Principal component analysis (PCA) of transcriptomes of *B. mori* brains in different developmental stages and *Met1* mosaics. First principal component (PC1) accounts for largest possible variance in dataset. Second principal component (PC2) was also calculated, under the condition that it is uncorrelated with (i.e., perpendicular to) PC1. Colors differentiate stages of domestic strain. Mutant and wild-type for 4th larval stage, L5D3: Third day of 5th instar larval stage; L5D6: Sixth day of 5th instar larval stage; W: Wandering stage; P0: Day 0 of pupal stage; P4: Day four of pupal stage; PP: Pre-pupal stage.

we carried out comparative transcriptional analysis of the two tissues in L4 WT and *Met1* mosaics. A total of 5.98–12.12 Gb of clean data were generated for each sample and 73.30%–82.10% of the total clean reads were mapped to the silkworm genome (Supplementary Table S2). We investigated the expression levels of selected representative JH and 20E responsive genes. As expected, the expression of *Kr-h1*, a responsive gene of JH signaling, was significantly down-regulated in the cuticle and brain of *Met1* mutants (Figure 3A, B). These results confirmed that the JH pathway was blocked in both the cuticle and brain of the mutants. In the mutant cuticle, the pupal-specifier gene *Br-C* (Kayukawa et al., 2016) and adult-specifier gene *E93* (Kayukawa et al., 2017) were significantly up-regulated (Figure 3A).

Epidermis and brain showed different transcriptomic pattern responses to *Met1* depletion

We generated comparative transcriptomic analyses between the WT and *Met1* mosaics in both the epidermis and brain.

There were 863 DEGs in the brain, nearly half the number found in the epidermis (1 523) (Figure 4A; Supplementary Tables S3, S4). A large proportion of DEGs (713, 82.6%) in the mutant brain were down-regulated (Figure 4A), possibly due to developmental arrest. In contrast, most DEGs were up-regulated in the epidermis (1 101, 72.3%), suggesting general gene activation in precocious metamorphosis.

The two sets of DEGs were enriched in different pathways. In the epidermis, DEGs were mainly enriched in metabolic pathways involved in sugar metabolism and amino acid biosynthesis (Figure 4B). Up- and down-regulated genes were present in the metabolic processes, indicating active dynamics of metabolism in the mutant epidermis (Figure 4B). In addition, melanin synthesis genes, which account for the formation of the brown-colored pupal cuticle (Wang et al., 2017), were up-regulated in the mutant epidermis (Supplementary Figure S3). These results indicate that the 20E-mediated pathways were triggered and functioned in the precocious pupation of the cuticle. Different from the active metabolic dynamics in the cuticle, enriched pathways in the brain were generally transcriptionally repressed, and included the highly enriched ECM-receptor interaction pathway, as well as the tyrosine metabolism, ABC transporter, retinol metabolism, and sugar metabolism pathways (Figure 4C). We compared the expression level of all genes in the ECM-receptor interaction pathway and found that they were markedly down-regulated in the mutant brain (Figure 4C). Protein digestion and absorption showed active dynamics, in contrast to active amino acid synthesis in the epidermis.

Artificial selection of *Met1* potentially affected protein structure and weakly regulated the *B. mori* network

We recently identified *Met1* as a candidate domestication gene in the domestic silkworm *B. mori* (Xiang et al., 2018). We confirmed the selection signature of *Met1* according to Xiang et al. (2018). The genomic region containing *Met1* demonstrated a strong selection signature with an elevated *F*st and *ROD* in the *B. mori* group (Figure 5A).

Based on the above evidence showing that *Met1* promotes silkworm larval brain development, and that the larval brain of domestic *B. mori* has fewer connections between the two lobes compared with wild *B. mandarina* (Figure 1), we further explored how artificial selection affected the biological function of *Met1* during silkworm brain domestication.

We found strong differentiation in allelic frequency of the *Met1* gene bodies (Figure 5A). Three nonsynonymous substitution sites showed high divergence in allelic frequency between the domestic (*B. mori*) and wild (*B. mandarina*) silkworms (Figure 5A, B). Residue 104 in the basic helix-loop-

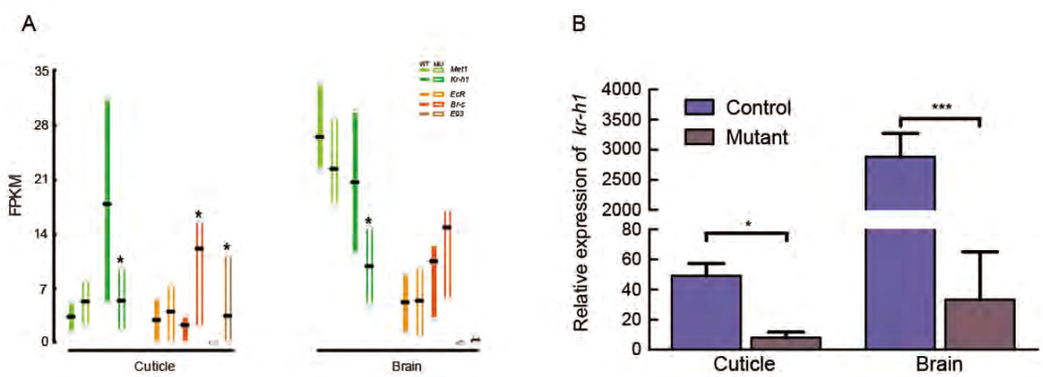

Figure 3 Gene expression gradient of representative genes of juvenile hormone (JH) and 20-hydroxyecdysone (20E) signaling pathways

A: Boxplot of gene expression showing that JH pathway is suppressed in both cuticle and brain of mutants. 20E pathway was up-regulated in cuticle of mutants, but there was no obvious change in the brain. WT: Wild-type; MU: Mutant; *EcR*: *Ecdysone Receptor*; *Brc*: *Broad-Complex*; *E93*: *Ecdysone-induced protein 93*; *Kr-h1*: *Krüppel homolog 1*. *EcR*, *Brc*, and *E93* are 20E responsive genes. *Kr-h1* is a JH-responsive gene. B: qRT-PCR validation of *Kr-h1* expression (n=3). Control: WT. Error bar: *SD*. WT refers to individuals from laboratory population of silkworm strain *Nistari*, which were not subjected to injection.

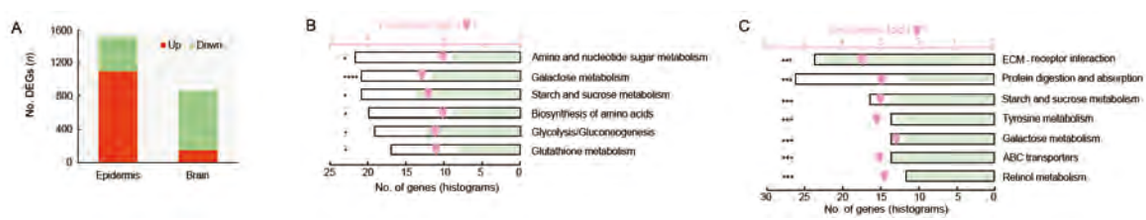

Figure 4 Illustration of comparative transcriptomics between *Met1* mosaics and wild-type (WT)

A: Numbers of DEGs between *Met1* mosaics and WT in brain and epidermis. B: All significantly enriched pathways corresponding to DEGs in epidermis between mutants and WT. C: All significantly enriched pathways corresponding to DEGs in brain between mutants and WT. Gene counts, down-regulated gene counts, and enrichment fold-levels are presented by black-framed blank histograms, shallow green-filled histograms, and heart-shaped symbols, respectively. Hypergeometric test (FDR-adjusted): *: P<0.05, ***: P<0.005, ****: P<0.001.

helix (bHLH) transcriptional activity domain and residue 210 in the region linking the two PAS domains (Charles et al., 2011) appeared to be under positive selection in the *B. mori* clade when compared with other Lepidoptera species, as detected by PAML analyses (Table 1). In the *B. mori* group, isoleucine and asparagine were relatively fixed at residues 104 and 210, respectively (Figure 5A, B), whereas all other Lepidoptera species carried valine and histidine, respectively (Figure 5B). The *B. mori* MET1 showed different 3D structure and protein dynamical properties in the region containing residue 210, where the imidazole-cycle bearing histidine conserved in other Lepidoptera species was replaced by aliphatic asparagine in the *B. mori* according to prediction (Figure 5C–E). These results suggest that mutations located in the linker region of the two PAS domains influenced the structure of MET1.

To further test the functional impact of the MET1 mutations, we conducted EMSA with *in vitro*-expressed MET1 proteins and the probe of the core binding region of its target gene *Kr-h1* (Kayukawa et al., 2012). We first tested the functional contribution of the linker region to MET1. Truncated MET1 without the linker region showed severely reduced binding activity with the labeled probes (Figure 6A), suggesting a key role of this region in transcriptional binding activity. We then compared the transcriptional binding activity of MET1 between *B. mori* and *B. mandarina*. Results indicated that MET1 had weaker binding activity with the labeled probe in *B. mori* than in *B. mandarina* (Figure 6A), suggesting that the *B. mori* allele in the linker region may contribute to the relatively weaker binding activity of MET1 as a transcription factor. In the competition assays, the specific band disappeared upon the addition of a 50- and 100-fold molar excess of unlabeled probe, indicating binding specificity.

To test whether the weaker binding activity of *B. mori* MET1 affects the downstream regulatory network of the silkworm larval brain, we combined unpublished brain transcriptome data from *B. mori* and *B. mandarina* to generate the weighted gene co-expression network module of *Met1* in both species (see Materials and Methods) (Figure 6B, C). There were fewer

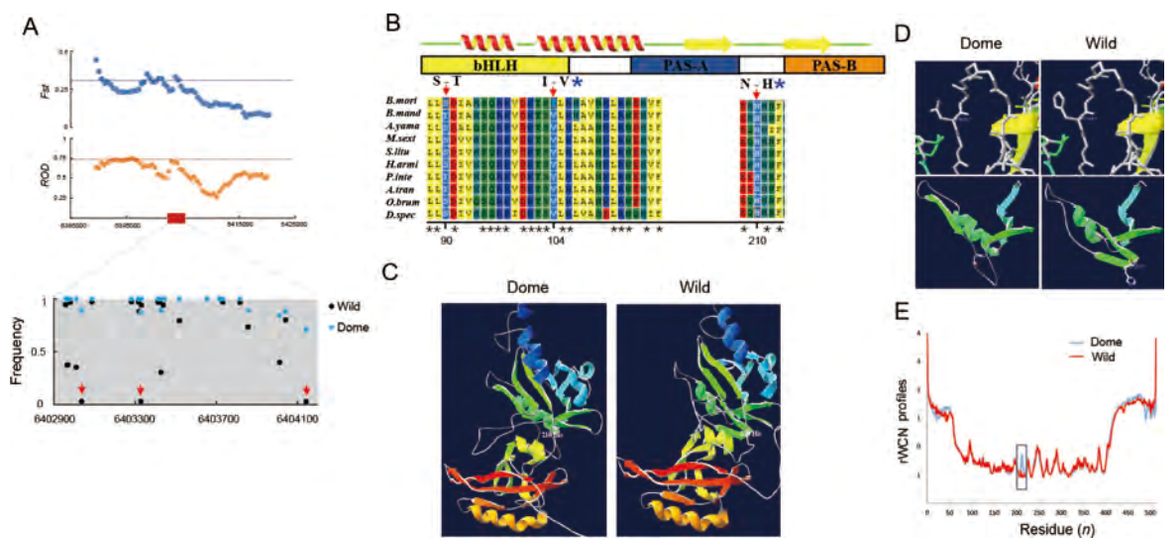

Figure 5 Selection of *Met1* and analysis of mutations

A: Selection of two independent sets of signatures of silkworm *Met1* *F*st and ROD between early domestication group (CHN_L_M3) of *B. mori* and *B. mandarina* is shown along genomic regions covering the *Met1* gene. Dashed lines represent top 5% of values. Plotting of frequency of reference genotype for each SNP position in coding region of *Met1* indicates many sites with obvious divergence in allelic frequency between *B. mandarina* and *B. mori* groups. Red arrow indicates three distinct SNP sites in coding region with nonsynonymous replacement. B: Sequence alignment of MET1 across 10 lepidopteran insects. Top shows distribution of secondary structure and functional domains. Red arrows indicate mutation sites S90T, I104V, and N210H, respectively. Blue stars indicate two sites appearing to be under positive selection in *B. mori*. Ten species are *B. mori*, *Bombyx mori*; *B. mand*, *Bombyx mandarina*; *A. yamamai*, *Antheraea yamamai*; *M. sext*, *Manduca sexta*; *S. litu*, *Spodoptera litura*; *H. armi*, *Helicoverpa armigera*; *P. inte*, *Plodia interpunctella*; *A. tran*, *Amyelois transitella*; *O. brum*, *Operophtera brumata*; *D. spec*, *Dendrolimus spectabilis*. C: Predicted 3D structures of MET1 in *B. mori* and *B. mandarina* allele. D: Detailed changes in predicted 3D structure of MET1 between *B. mori* and *B. mandarina* allele in the region covering residue 210. E: Protein dynamical properties of MET1 of *B. mandarina* and *B. mori* allele, indicating a remarkable difference in the position of residue 210.

Table 1 PAML analysis of *Met1* in Lepidoptera species

Model	ω0	ω1(target)	ω background	2Δ*l*	*P*-value	Positive site (possibility ω>1)	lnL
Null (one ratio)	0.0455						–9625.72
2-ratio (*B. mori* vs. other)		999	0.044 00	3.40	0.060 0		–9624.02
2-ratio (branch site, *B. mori* vs. other)				115.80	0.000 0	122 I (0.933); 229 N (0.948)	–9567.82

lnL: Likelihood; Positive sites were identified by Bayes Empirical Bayes analysis.

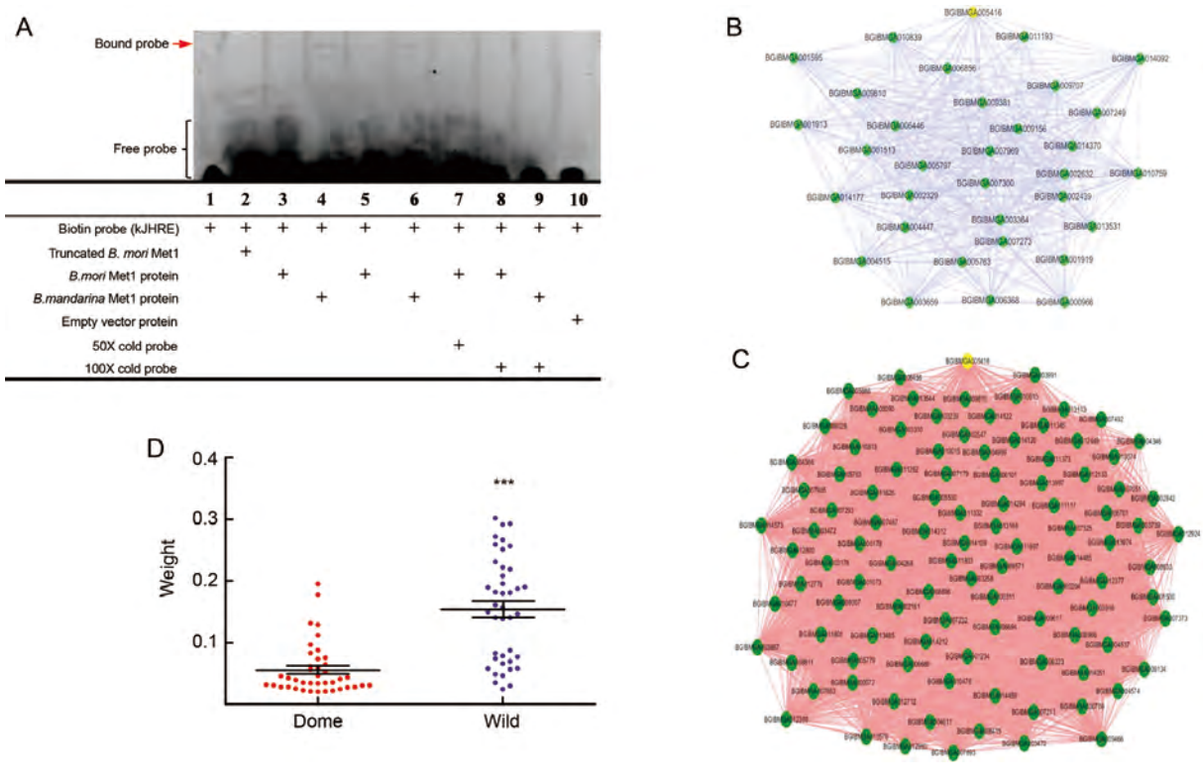

Figure 6 Influence of MET1 mutation on binding activity as a transcription factor and on co-expressed genes identified by weighted correlation network analysis (WGCNA)

A: Electrophoretic mobility shift assay. *In vitro* expressed MET1 protein was used to bind to the core region of the kJHRE probe at 24 bp (GCGGTGGGCCTCCACGTGTCGAACG) in the *Kr-h1* promoter, repeated twice. Competition assays were performed using 50- and 100-fold molar excesses of unlabeled specific probes. Concentration of polyacrylamide gel was 6%. Truncated *B. mori* Met1 indicates truncated MET1 protein without a linker region between the two PAS domains. B, C: Gene co-expression network of *Met1* located modules in the brains of *B. mori* (B) and *B. mandarina* (C) *BGIBMGA005416*, *Met1*. Each node represents a probe, and each line denotes gene expression correlation between two nodes. D: Comparison of connection weight of co-expressed genes with *Met1* in *B. mori* and *B. mandarina*.

genes co-expressed with *Met1* in *B. mori* (Figure 6B) than in *B. mandarina* (Figure 6C). Also, the connection weight between those genes and *Met1* was significantly lower in *B. mori* than in *B. mandarina* (Figure 6D). A weak co-expression network has also been reported in cultivated maize compared with its wild ancestor (Swanson-Wagner et al., 2012), implying that this mechanism may be common during rapidly evolved domestication. We suspect that the weak binding activity of *B. mori Met1* may be associated with a weakened regulatory network in the brain during silkworm domestication. Whether and how this affects brain volume during silkworm domestication still needs further exploration.

Tyrosine metabolism pathway affected by JH signaling via *Met1* may be involved in silkworm larval brain development and domestication

To further explore potential *Met1*-affected transcriptomic changes in the larval brain during silkworm domestication, we performed comparative brain transcriptomic analyses between *B. mori* and *B. mandarina* at three larval stages (Figure 1). We obtained 6.15–12.12 Gb of clean data for each sample (Supplementary Table S2). In total, 1 848, 3 953, and 2 962 DEGs were identified between *B. mori* and *B. mandarina* in the middle of the final larval stage, end of the final larval stage, and wandering stage, respectively (Supplementary Tables S5–S7). Almost no significantly enriched pathways were identified (Supplementary Table S8), but the tyrosine metabolism, ABC transporter, galactose metabolism, and ECM-receptor interaction pathways, which were enriched in the DEGs between the mutant vs. WT comparison (Figure 4C), were among the top ranked (but non-significant) enrichment results (Supplementary Table S8). We further overlapped two sets of DEGs, i.e., mutant vs. WT and *B. mori* vs. *B. mandarina*, at the three larval stages, respectively, and performed KEGG enrichment analyses of the shared DEGs for each group. Notably, tyrosine metabolism was the common enriched pathway at the three larval stages (Figure 7A), suggesting that this pathway is involved in both larval brain development and domestication.

We investigated two core pathways in the tyrosine metabolism network (Figure 7B). One pathway involved the catalysis of tyrosine by peroxidase (POD) and peroxidasin (PXDN) to form tyrosine derivatives (Figure 7B). These two enzymes can generate tyrosine-tyrosine bonds to stabilize the ECM (Fessler et al., 1994). In the brain of *Met1* mosaics, the DEGs encoding the two enzymes were all down-regulated (Figure 7B; Supplementary Figure S4), suggesting that depletion of JH signaling influenced the ECM of the brain

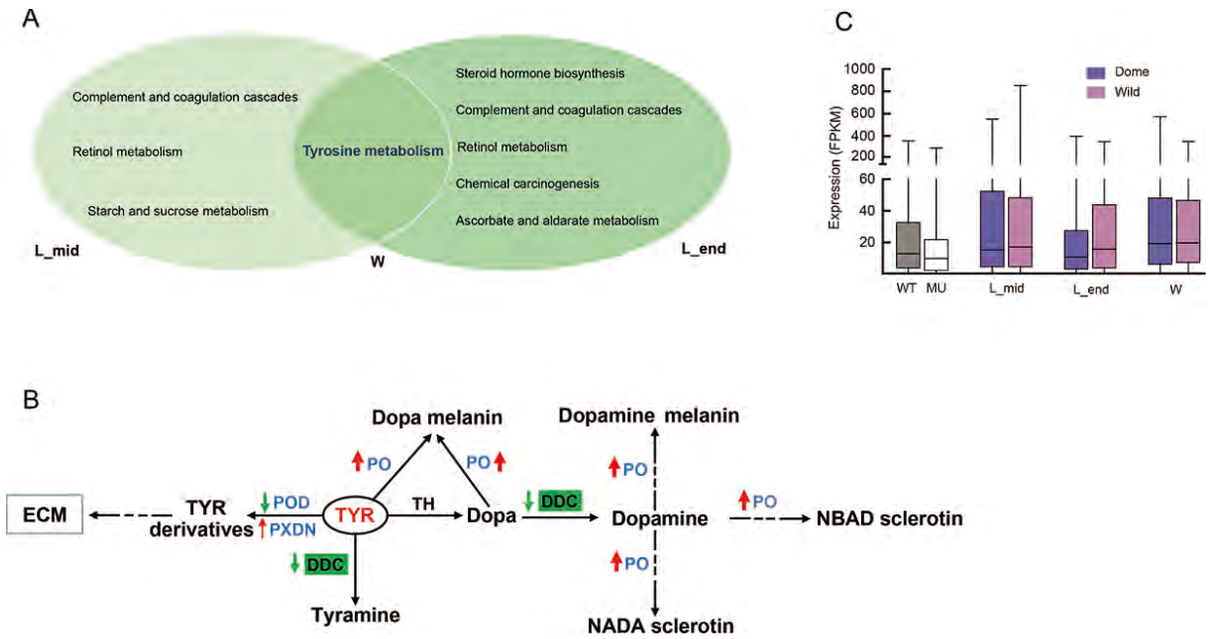

Figure 7 Illustration of comparative transcriptomics between *B. mori* and *B. mandarina*

A: Venn diagram of enriched pathways corresponding to common DEGs in mutant compared to WT and *B. mori* compared to *B. mandarina* at three larval stages. KEGG enrichment in these DEGs indicated that tyrosine metabolism is a common pathway. Redundant and human disease items were removed. L_mid: Middle of final larval stage; L_end: Final day of final larval stage; W: Wandering stage. B: Two core pathways in tyrosine metabolic network. Proteins in blue are coded by DEGs in both mutant vs. WT and *B. mori* vs. *B. mandarina* at three larval stages, and these genes were all down-regulated in mutants. TYR: Tyrosine; NADA: N-acetyl dopamine; NBAD: N-b-alanyl dopamine; PO: Phenoloxidases. DDC: Dopa decarboxylase. Genes with green background represent down-regulated genes specific in *B. mori* vs. *B. mandarina*. Relationship to ECM was obtained from the literature. Red and green arrows indicate that genes were up- and down-regulated in *B. mori* compared to *B. mandarina*, respectively. Arrow weight represents number of genes. C: Boxplot of gene expression in ECM-receptor interaction pathway. WT: Wild-type; MU: Mutant; Wild: *B. mandarina*; Dome: *B. mori*. WT refers to individuals from laboratory population of domestic silkworm strain *Nistari*, which were not subjected to injection.

(Figure 4C). Genes encoding *Pod* in the *B. mori* brain were down-regulated compared with that in *B. mandarina* (Figure 7B; Supplementary Figure S4). However, when we compared the expression of all genes involved in the ECM-receptor pathway, we found no differential expression in the brain between *B. mori* and *B. mandarina* (Figure 7C).

The other pathway is the tyrosine-tyramine and dopamine-pigmentation melanin synthesis pathway (Figure 7B). The three shared DEGs encode phenoloxidases (POs), which are at the distal end in melanin synthesis (Wang et al., 2017). They are involved in insect immunity and are considered important enzymes in the insect developmental process. For example, in the oriental fruit fly, RNAi knockdown of PO at the end larval stage impedes larval-pupal transition (Bai et al., 2014). Here, genes encoding PO in the *Met1* mutant brain were also down-regulated (Figure 7B), suggesting roles in brain development. Interestingly, genes encoding PO were up-regulated in the *B. mori* brain compared to the *B. mandarina* brain (Figure 7B) and DOPA decarboxylases (DDCs) were specifically down-regulated in *B. mori* (Figure 7B; Supplementary Figure S4). DDCs use tyrosine and L-dopa as substrates to synthesize tyramine and dopamine, respectively. Up-regulated POs and down-regulated DDCs may have resulted in a deficiency of tyramine and/or dopamine in *B. mori* compared with *B. mandarina*.

DISCUSSION

By generating mosaic loss-of-function mutants of the JH receptor *Met1*, we demonstrated that JH signaling promotes the development of the silkworm larval brain. However, this promotion could not be simply explained by repression of precocious metamorphosis, which is easily detected in the epidermis (Daimon et al., 2015; Zhu et al., 2019). Firstly, we found that the *Met1* mutant epidermis showed active dynamics of sugar metabolism and amino acid biosynthesis, which usually occur in tissues experiencing metamorphosis, whereas gene expression was largely repressed in the brain. Secondly, expression of the JH-responsive gene *Kr-h1* was down-regulated in both the epidermis and brain, whereas the genes related to metamorphosis (i.e., *Br-C* and *E93*) were only up-regulated in the epidermis, thus confirming the different responses of the two tissues to *Met1* defects. Further exploration of JH and *Kr-h1* should improve our understanding of the regulation role of JH signaling in silkworm brain development. Thirdly, we identified several downstream pathways that *Met1* may affect in the brain, including the ECM-receptor interaction and tyrosine metabolism pathways. The ECM consists of many families of molecules, including collagens, non-collagenous glycoproteins, glycosaminoglycans, and proteoglycans, and plays an important role in processes underlying the development, maintenance, and

regeneration of the nervous system (Broadie et al., 2011). Here, down-regulation of this pathway in the silkworm mutant brain resulted in developmental arrest of the larval brain. In regard to the tyrosine metabolism pathway, which was generally repressed in the *Met1* mutants, we noted that a branch in this pathway, i.e., catalysis of tyrosine by POD and PXDN to form tyrosine derivatives, is related to the biosynthesis of thyroxine and its derivatives (Wang et al., 2017) (Supplementary Figure S5). In mammals, thyroxine is a very important hormone secreted by the thyroid and coordinates with growth hormone to regulate brain development (Roger & Fellows, 1979). While earlier studies have suggested that derivatives of thyroxine can mimic the effects of JH to influence egg production in some insects (Kim et al., 1999), whether this biosynthesis pathway is active in insects remains unknown, raising the question of the role of this hormone in the insect brain. On the other hand, the POD and PXDN enzymes can generate tyrosine-tyrosine bonds, which stabilize the ECM (Fessler et al., 1994), suggesting that the ECM-receptor interaction and tyrosine metabolism pathways may interact.

Based on molecular evolution, functional assay of potential causal replacement in *Met1*, and comparative brain transcriptome analyses between *B. mori* and *B. mandarina*, we explored the possible mechanism and biological impact of artificial selection on this domestication gene. We identified a novel motif of MET1 that may influence its function as a transcription factor and detected a notable amino acid replacement in this motif fixed in *B. mori* during the domestication process. The amino acid replacement was predicted to affect the 3D protein structure and dynamic characteristics. Intriguingly, despite large-scale evolution in Lepidoptera, this replacement was still only specific in the domestic species, with a strong positive selection signature. All other tested wild species uniformly showed the other genotype at this site. We suspect that this artificially selected replacement may have had substantial biological impact on the adaptation of wild silkworms to the domestic environment. In domestic dogs, Axelsson et al. (2013) also identified candidate mutations in key genes of the starch digestion pathway, which showed higher catalytic activity, with some of these mutations also shared in herbivores. Our results suggested that the *Met1* mutation in *B. mori* may result in weaker binding activity to the *cis*-element of the JH-responsive gene *Kr-h1*, and further influence the regulatory network. Evidence from crops suggests that modifications in transcription factors play important roles in domestication and affect agronomic traits in a pleiotropic manner (Gross & Olsen, 2010). Here, the biological impact of the artificial selection of *Met1* also influenced multiple aspects of silkworm domestication. JH-*Met1*-*Kr-h1* signaling functions in multiple tissues and shows complex crosstalk with other signaling pathways, and varies among tissues and species (Li et al., 2019; Riddiford, 2020; Shpigler et al., 2020). In the brain, we detected a weaker co-expression network of *Met1* in *B. mori* than in *B. mandarina*. Although this predicted network requires further verification, it provides a preliminary landscape of the impact of *Met1* artificial selection on brain gene expression patterns, which may further influence the development of the brain itself and the behaviors that the brain controls.

In the larval brain, comprehensive transcriptomic analyses indicated that tyrosine metabolism was a potential downstream pathway influenced by artificial selection of JH signaling. Its intermediate products, i.e., tyramine and dopamine, are important brain neurotransmitters and affect invertebrate behaviors such as locomotion, nutritional state, escape response, and flight (Riemensperger et al., 2011; Schützler et al., 2019; Vierk et al., 2009). For instance, in *Drosophila*, deficiency of dopamine results in reduced activity, extended sleep time, locomotor deficits, and hyperphagia, similar to that found in *B. mori* compared to *B. mandarina*. Previous research has reported that JH regulates these brain biogenic amine systems (Zhu et al., 2009). Therefore, we propose that artificial selection of JH signaling may have acted on tyrosine metabolism, thereby influencing the brain biogenic amine system, at least for larval behavioral changes, during silkworm domestication.

DATA AVAILABILITY

RNA-seq data were deposited in the NCBI under BioProjectID PRJNA756861 and were deposited in the Genome Sequence Archive (GSA) database under Accession No. CRA004783.

SUPPLEMENTARY DATA

Supplementary data to this article can be found online.

COMPETING INTERESTS

The authors declare that they have no competing interests.

AUTHORS' CONTRIBUTIONS

Y.C. performed the experiments, collected and analyzed the data, and wrote the paper; Z.L.L. and L.Y. performed the microinjections; Y.J.L. performed resource collection; C.C.L., Z.D.Z., X.M.W., and H.M.D. participated in data analysis; H.X., Y.P.H., and Q.L.F. designed the experiment, analyzed the data, and wrote the manuscript. All authors read and approved the final version of the manuscript.

ACKNOWLEDGEMENTS

We thank Dr. An-Jiang Tan for the Cas9 gene template used in this work, Dr. Shuai Zhan for help in genomic data analyses, Yu-Ling Peng for help with microinjections, and Dr Mu-Wang Li for help in silkworm maintenance. We thank LetPub (www.letpub.com) for linguistic assistance during the preparation of this manuscript.

REFERENCES

Abdou MA, He QY, Wen D, Zyaan O, Wang J, Xu JJ, et al. 2011. *Drosophila* Met and Gce are partially redundant in transducing juvenile hormone action. *Insect Biochemistry and Molecular Biology*, **41**(12): 938−945.

Agnvall B, Bélteky J, Jensen P. 2017. Brain size is reduced by selection for tameness in Red Junglefowl-correlated effects in vital organs. *Scientific Reports*, **7**(1): 3306.

Anders S, Pyl PT, Huber W. 2015. HTSeq—a Python framework to work

with high-throughput sequencing data. *Bioinformatics*, **31**(2): 166−169.
Axelsson E, Ratnakumar A, Arendt ML, Maqbool K, Webster MT, Perloski M, et al. 2013. The genomic signature of dog domestication reveals adaptation to a starch-rich diet. *Nature*, **495**(7441): 360−364.
Bai PP, Xie YF, Shen GM, Wei DD, Wang JJ. 2014. Phenoloxidase and its zymogen are required for the larval-pupal transition in *Bactrocera dorsalis* (Diptera: Tephritidae). *Journal of Insect Physiology*, **71**: 137−146.
Broadie K, Baumgartner S, Prokop A. 2011. Extracellular matrix and its receptors in *drosophila* neural development. *Developmental Neurobiology*, **71**(11): 1102−1130.
Cayre M, Malaterre J, Scotto-Lomassese S, Aouane A, Strambi C, Strambi A. 2005. Hormonal and sensory inputs regulate distinct neuroblast cell cycle properties in adult cricket brain. *Journal of Neuroscience Research*, **82**(5): 659−664.
Cayre M, Strambi C, Strambi A. 1994. Neurogenesis in an adult insect brain and its hormonal control. *Nature*, **368**(6466): 57−59.
Champlin DT, Truman JW. 1998. Ecdysteroid control of cell proliferation during optic lobe neurogenesis in the moth *Manduca sexta*. *Development*, **125**(2): 269−277.
Charles JP, Iwema T, Epa VC, Takaki K, Rynes J, Jindra M. 2011. Ligand-binding properties of a juvenile hormone receptor, Methoprene-tolerant. *Proceedings of the National Academy of Sciences of the United States of America*, **108**(52): 21128−21133.
Cui Y, Zhu YA, Lin YJ, Chen L, Feng QL, Wang W, et al. 2018. New insight into the mechanism underlying the silk gland biological process by knocking out fibroin heavy chain in the silkworm. *BMC Genomics*, **19**(1): 215.
Daimon T, Kozaki T, Niwa R, Kobayashi I, Furuta K, Namiki T, et al. 2012. Precocious metamorphosis in the juvenile hormone-deficient mutant of the silkworm, *Bombyx mori*. *PLoS Genetics*, **8**(3): e1002486.
Daimon T, Uchibori M, Nakao H, Sezutsu H, Shinoda T. 2015. Knockout silkworms reveal a dispensable role for juvenile hormones in holometabolous life cycle. *Proceedings of the National Academy of Sciences of the United States of America*, **112**(31): E4226−E4235.
Ezure T, Suzuki T, Shikata M, Ito M, Ando E. 2010. A cell-free protein synthesis system from insect cells. *Methods in Molecular Biology*, **607**: 31−42.
Fessler LI, Nelson RE, Fessler JH. 1994. *Drosophila* extracellular matrix. *Methods in Enzymology*, **245**: 271−294.
Fu YF, Sander JD, Reyon D, Cascio VM, Joung JK. 2014. Improving CRISPR-Cas nuclease specificity using truncated guide RNAs. *Nature Biotechnology*, **32**(3): 279−284.
Ghosh S, Chan CK. 2016. Analysis of RNA-seq data using TopHat and cufflinks. *Methods in Molecular Biology*, **1374**: 339−361.
Golan-Mashiach M, Grunspan M, Emmanuel R, Gibbs-Bar L, Dikstein R, Shapiro E. 2012. Identification of CTCF as a master regulator of the clustered protocadherin genes. *Nucleic Acids Research*, **40**(8): 3378−3391.
Gross BL, Olsen KM. 2010. Genetic perspectives on crop domestication. *Trends in Plant Science*, **15**(9): 529−537.
Guex N, Peitsch MC. 1997. SWISS-MODEL and the Swiss-Pdb Viewer: an environment for comparative protein modeling. *Electrophoresis*, **18**(15): 2714−2723.
Huang TT, Hwang JK, Chen CH, Chu CS, Lee CW, Chen CC. 2015. $(PS)^2$: protein structure prediction server version 3.0. *Nucleic Acids Research*, **43**(W1): W338−W342.
Hwang WY, Fu YF, Reyon D, Maeder ML, Tsai SQ, Sander JD, et al. 2013. Efficient genome editing in zebrafish using a CRISPR-Cas system. *Nature Biotechnology*, **31**(3): 227−229.
Kanost MR, Arrese EL, Cao XL, Chen YR, Chellapilla S, Goldsmith MR, et al. 2016. Multifaceted biological insights from a draft genome sequence of the tobacco hornworm moth, *Manduca sexta*. *Insect Biochemistry and Molecular Biology*, **76**: 118−147.
Kayukawa T, Minakuchi C, Namiki T, Togawa T, Yoshiyama M, Kamimura M, et al. 2012. Transcriptional regulation of juvenile hormone-mediated induction of Krüppel homolog 1, a repressor of insect metamorphosis. *Proceedings of the National Academy of Sciences of the United States of America*, **109**(29): 11729−11734.
Kayukawa T, Nagamine K, Ito Y, Nishita Y, Ishikawa Y, Shinoda T. 2016. Krüppel homolog 1 inhibits insect metamorphosis via direct transcriptional repression of *Broad-Complex*, a pupal specifier gene. *Journal of Biololgical Chemisty*, **291**(4): 1751−1762.
Kayukawa T, Jouraku A, Ito Y, Shinoda T. 2017. Molecular mechanism underlying juvenile hormone-mediated repression of precocious larval-adult metamorphosis. *Proceedings of the National Academy of Sciences of the United States of America*, **114**(5): 1057−1062.
Kim SR, Kwak W, Kim H, Caetano-Anolles K, Kim KY, Kim SB, et al. 2018. Genome sequence of the Japanese oak silk moth, *Antheraea yamamai*: the first draft genome in the family Saturniidae. *Gigascience*, **7**(1): gix113.
Kim Y, Davari ED, Sevala V, Davey KG. 1999. Functional binding of a vertebrate hormone, L-3,5,3'-triiodothyronine (T_3), on insect follicle cell membranes. *Insect Biochemistry and Molecular Biology*, **29**(10): 943−950.
Langfelder P, Horvath S. 2008. WGCNA: an R package for weighted correlation network analysis. *BMC Bioinformatics*, **9**(1): 559.
Leinwand SG, Scott K. 2021. Juvenile hormone drives the maturation of spontaneous mushroom body neural activity and learned behavior. *Neuron*, **109**(11): 1836−1847.e5.
Li K, Jia QQ, Li S. 2019. Juvenile hormone signaling - a mini review. *Insect Science*, **26**(4): 600−606.
Li M, Li DY, Tang Y, Wu FX, Wang JX. 2017. CytoCluster: a cytoscape plugin for cluster analysis and visualization of biological networks. *International Journal of Molecular Sciences*, **18**(9): 1880.
Lin CP, Huang SW, Lai YL, Yen SC, Shih CH, Lu CH, et al. 2008. Deriving protein dynamical properties from weighted protein contact number. *Proteins*, **72**(3): 929−935.
Liu SN, Li K, Gao Y, Liu X, Chen WT, Ge W, et al. 2018. Antagonistic actions of juvenile hormone and 20-hydroxyecdysone within the ring gland determine developmental transitions in *Drosophila*. *Proceedings of the National Academy of Sciences of the United States of America*, **115**(1): 139−144.
Love MI, Huber W, Anders S. 2014. Moderated estimation of fold change and dispersion for RNA-seq data with DESeq2. *Genome Biology*, **15**(12): 550.
Mignon-Grasteau S, Boissy A, Bouix J, Faure JM, Fisher AD, Hinch GN, et al. 2005. Genetics of adaptation and domestication in livestock. *Livestock Production Science*, **93**(1): 3−14.
Nusinovich Y, Ucko S, Ucko H. 2017. How to tame a fox (and Build a Dog): visionary scientists and a siberian tale of jump-started evolution. *Science*, **358**(6368): 1250−1250.
Pennisi E. 2011. The biology of genomes. *On the trail of brain domestication genes. Science*, **332**(6033): 1030−1031.
Riddiford LM. 2020. *Rhodnius*, golden oil, and *Met*: a history of juvenile hormone research. *Frontiers in Cell and Developmental Biology*, **8**: 679.
Riddiford LM, Truman JW, Mirth CK, Shen YC. 2010. A role for juvenile

hormone in the prepupal development of *Drosophila melanogaster*. *Development*, **137**(7): 1117−1126.

Riemensperger T, Isabel G, Coulom H, Neuser K, Seugnet L, Kume K, et al. 2011. Behavioral consequences of dopamine deficiency in the *Drosophila* central nervous system. *Proceedings of the National Academy of Sciences of the United States of America*, **108**(2): 834−839.

Roger LJ, Fellows RE. 1979. Evidence for thyroxine-growth hormone interaction during brain development. *Nature*, **282**(5737): 414−415.

Sasaki K, Akasaka S, Mezawa R, Shimada K, Maekawa K. 2012. Regulation of the brain dopaminergic system by juvenile hormone in honey bee males (*Apis mellifera* L.). *Insect Molecular Biology*, **21**(5): 502−509.

Schützler N, Girwert C, Hügli I, Mohana G, Roignant JY, Ryglewski S, et al. 2019. Tyramine action on motoneuron excitability and adaptable tyramine/octopamine ratios adjust *Drosophila* locomotion to nutritional state. *Proceedings of the National Academy of Sciences of the United States of America*, **116**(9): 3805−3810.

Shpigler HY, Herb B, Drnevich J, Band M, Robinson GE, Bloch G. 2020. Juvenile hormone regulates brain-reproduction tradeoff in bumble bees but not in honey bees. *Hormones and Behavior*, **126**: 104844.

Stuermer IW, Wetzel W. 2006. Early experience and domestication affect auditory discrimination learning, open field behaviour and brain size in wild Mongolian gerbils and domesticated laboratory gerbils (*Meriones unguiculatus* forma domestica). *Behavioural Brain Research*, **173**(1): 11−21.

Swanson-Wagner R, Briskine R, Schaefer R, Hufford MB, Ross-Ibarra J, Myers CL, et al. 2012. Reshaping of the maize transcriptome by domestication. *Proceedings of the National Academy of Sciences of the United States of America*, **109**(29): 11878−11883.

Tan AJ, Fu GL, Jin L, Guo QH, Li ZQ, Niu BL, et al. 2013. Transgene-based, female-specific lethality system for genetic sexing of the silkworm, *Bombyx mori*. *Proceedings of the National Academy of Sciences of the United States of America*, **110**(17): 6766−6770.

Tanriverdi OE, Yelkovan S. 2020. Histological investigation of the effects of fenoxycarb on neurosecretory cells in the silkworm, *Bombyx mori* brain. *Invertebrate Neuroscience*, **20**(4): 20.

Tamura K, Stecher G, Peterson D, Filipski A, Kumar S. 2013. MEGA6: Molecular Evolutionary Genetics Analysis Version 6.0. *Molecular Biology and Evolution*, **30**(12): 2725−2729.

Trapnell C, Pachter L, Salzberg SL. 2009. TopHat: discovering splice junctions with RNA-Seq. *Bioinformatics*, **25**(9): 1105−1111.

Trapnell C, Williams BA, Pertea G, Mortazavi A, Kwan G, van Baren MJ, et al. 2010. Transcript assembly and quantification by RNA-Seq reveals unannotated transcripts and isoform switching during cell differentiation. *Nature Biotechnology*, **28**(5): 511−515.

Vierk R, Pflueger HJ, Duch C. 2009. Differential effects of octopamine and tyramine on the central pattern generator for *Manduca* flight. *Journal of Comparative Physiology A*, **195**(3): 265−277.

Wang MS, Zhang RW, Su LY, Li Y, Peng MS, Liu HQ, et al. 2016. Positive selection rather than relaxation of functional constraint drives the evolution of vision during chicken domestication. *Cell Research*, **26**(5): 556−573.

Wang PY, Qiu ZY, Xia DG, Tang SM, Shen XJ, Zhao QL. 2017. Transcriptome analysis of the epidermis of the *purple quail-like* (*q-l*^{p}) mutant of silkworm, *Bombyx mori*. *PLoS One*, **12**(4): e0175994.

Wheeler MM, Ament SA, Rodriguez-Zas SL, Southey B, Robinson GE. 2015. Diet and endocrine effects on behavioral maturation-related gene expression in the pars intercerebralis of the honey bee brain. *Journal of Experimental Biology*, **218**(Pt 24): 4005−4014.

Xiang H, Liu XJ, Li MW, Zhu YN, Wang LZ, Cui Y, et al. 2018. The evolutionary road from wild moth to domestic silkworm. *Nature Ecology & Evolution*, **2**(8): 1268−1279.

Yang Z. 1997. PAML: a program package for phylogenetic analysis by maximum likelihood. *Computer Applications in the Biosciences*, **13**(5): 555−556.

Yang ZH, Wong WSW, Nielsen R. 2005. Bayes empirical bayes inference of amino acid sites under positive selection. *Molecular Biology and Evolution*, **22**(4): 1107−1118.

Zhu GH, Jiao YY, Chereddy SCRR, Noh MY, Palli SR. 2019. Knockout of juvenile hormone receptor, Methoprene-tolerant, induces black larval phenotype in the yellow fever mosquito, *Aedes aegypti*. *Proceedings of the National Academy of Sciences of the United States of America*, **116**(43): 21501−21507.

Zhu HS, Gegear RJ, Casselman A, Kanginakudru S, Reppert SM. 2009. Defining behavioral and molecular differences between summer and migratory monarch butterflies. *BMC Biology*, **7**(1): 14.